Assessment of the Damage Tolerance of Postbuckled Hat-Stiffened Panels using Single-Stringer Specimens

Chiara Bisagni[1] and Riccardo Vescovini[2]
Politecnico di Milano, Milano 20156, Italy

and

Carlos G. Dávila[3]
NASA Langley Research Center, Hampton, VA 23681

A procedure is proposed for the assessment of the damage tolerance and collapse of stiffened composite panels using a single-stringer compression specimen. The dimensions of the specimen are determined such that the specimen's nonlinear response and collapse are representative of an equivalent multi-stringer panel in compression. Experimental tests are conducted on specimens with and without an embedded delamination. A shell-based finite element model with intralaminar and interlaminar damage capabilities is developed to predict the postbuckling response as well as the damage evolution from initiation to collapse.

I. Introduction

Major gains in structural efficiency can be achieved by exploiting the ability of stiffened composite structures to operate deep into the postbuckling field. Unfortunately, these potential weight savings are not yet completely achievable, mainly because of the difficulty in determining the durability and damage tolerance of postbuckled structures. Consequently, the increasing interest in the study of damage tolerant structures has stimulated the development of new tools able to describe complex structural responses such as damage propagation[1-4] and delamination[5-7].

The design and certification of composite structures is usually conducted by following a chronological sequence of progressively more complex structural evaluations called the Building Block Approach. This approach starts with a large number of coupon tests for the establishment of material database, and it progresses across specimens and components of increasing complexity. However, a gap still exists between the coupon tests used for material characterization and the structural tests needed for panel response, such as those conducted on stiffened panels[8-13] or on closed box configurations[14-15]. In a previous paper by the authors[16], the use of a simple specimen consisting of one L-shaped stringer bonded to the skin was proposed for the study of skin-stringer separation with the virtual crack closure technique. The collapse and degradation of blade-stiffened panels have also been studied with a global-local analysis technique both on single-stringer specimens[17] and on multi-stringer configurations[18].

In the present work, the response of single-stringer compression (SSC) specimens with a co-cured hat-stringer is investigated. These specimens were designed and manufactured at the Politecnico di Milano for the evaluation of the structural integrity of stiffened structures. The SSC specimens represent a level of complexity that can bridge the gap between coupon specimens and structural components. Their small size, the relative complexity and low manufacturing cost are ideal for assessing the effects of manufacturing defects and impact damage on the integrity

---

[1] Associate Professor, Department of Aerospace Engineering, Via La Masa 34, chiara.bisagni@polimi.it, AIAA Member.
[2] Ph.D. student, Department of Aerospace Engineering, Via La Masa 34, vescovini@aero.polimi.it.
[3] Aerospace Research Engineer, Structural Mechanics and Concepts Branch, NASA LaRC, Hampton, VA, carlos.g.davila@nasa.gov, AIAA Senior Member.

of composite structures subjected to compression loads. The damage tolerance of SSC specimens is investigated by placing a Teflon insert between the stringer and the skin insert during manufacturing.

Since the SSC specimens are relatively small, computationally tractable yet detailed damage models can be constructed to account for all damage modes: matrix cracking, fiber kinking, fiber fracture, and delamination. Therefore, the test results of these specimens are also ideal for validating or redefining aspects of state-of-the-art damage models, and in particular the modeling and numerical issues related to compression failure and structural collapse. In the present study, damage models developed as Abaqus user-written subroutines have been used[3-7]. Consequently, the dual objective of the present work is to propose a methodology for the development of SSC specimens that are representative of the response of stiffened panels and to use the experimental results to validate the predictions made using the progressive damage analysis tools.

II. Single-Stringer Compression Specimen

Aeronautical panels are stiffened with stringers in the axial direction and with frames in the circumferential direction. A typical fuselage structure is shown in Fig. 1, where stringers with hat section are clearly visible. The stringer configuration influences both the buckling and postbuckling behavior as well as the damage and collapse mechanisms.

Typical aeronautical structures can sustain loads much higher than the initial buckling load, which usually consists of local buckling of the skin. Postbuckling loads can be carried through internal load re-distribution, accompanied by a higher ratio of load sustained by the stiffeners. As the load increases, the stiffeners can also undergo local buckling modes with a consequent loss of stiffness.

The buckling of open-section stiffeners generally induces a loss of stiffness that may lead the stringer to twist and bend, which can trigger a global buckling mode. The failure is usually governed by interlaminar damage mechanisms induced by the out-of-plane postbuckling deformation, while intralaminar damage mechanisms are activated during the structural collapse.

Figure 1. Typical composite fuselage.

On the other hand, local buckling of closed-section stringers such as hat stringers can happen at loads that are significantly lower than the global buckling load. In this case, the panel generally collapses by crippling, with failure modes involving both interlaminar and intralaminar damage mechanisms. In the case of multi-stringer panels, the complexity of the interaction between these nonlinear responses renders their prediction computationally impractical.

For computational efficiency and also for experimental considerations, a single-stringer hat specimen was developed based on the geometrically nonlinear analysis of a multi-stringer panel. By identifying repeating features that characterize the response of a multi-stringer panel, it is possible to determine the dimensions of a single-stringer specimen whose response is similar to that of the multi-stringer panel in terms of postbuckling deformation and failure mechanisms.

The multi-stringer panel under investigation is composed of five stringers. The panel has a total length of 720 *mm*, a width of 680 *mm* and a stringer pitch of 152 *mm*. The height of the stringers is 30 *mm*, the width of the crown top is 15 *mm*, while the web angle measured from the normal to the skin is equal to 25°. The stringers are bonded to the skin along two 15 *mm*-wide flanges. Both the skin and the stringers are made from IM7/8552 graphite-epoxy material.

The skin consists of an 8-ply quasi-isotropic laminate with a stacking sequence of $[45°/90°/-45°/0°]_S$ for a total thickness of 1 *mm*. The stringers are composed of a 7-ply laminate with a symmetric stacking sequence of [-45°/0°/45°/0°/45°/0°/-45°] which results in a total thickness of 0.875 *mm*. The skin and stringer are co-cured.

The starting point of the design of the SSC specimen is a finite element model of a multi-stringer panel. A quasi-static postbuckling analysis is performed to determine repeating patterns of stresses and deformation. The dimensions of the SSC specimen are determined to ensure a similar deformation pattern in terms of number of half-

waves, and consequently a similar bending stress distribution on the skin. The similarity in the stress field also guarantees a similarity in the interaction between the skin and the stringer in terms of rotations and bending moments that may induce skin/stringer separation.

The complete panel has a deformed pattern consisting of one half-wave between stringers and 11-12 half-waves in the longitudinal direction (Fig. 2a). The periodicity of the deformation pattern also dictates a periodicity in the stress and strain distribution, so the main failure mechanisms involved in the collapse of the structure are present in each of the repeating units. A structure sub-unit identified by an area characterized by three half-waves along the longitudinal direction is shown in Fig. 2b, where the color contours represent the maximum stress criterion.

The sizing of the SSC specimen is performed by studying nine different configurations, where the width is varied from 130 *mm* to 170 *mm*, and the length from 220 *mm* to 260 *mm*, in 20-*mm* increments. All nine configurations are characterized by a buckling mode with three half-waves along the longitudinal direction. Among them, the configuration that best represents the distribution of the maximum stress criterion is the one with length of 240 *mm* and width of 150 *mm*, which is approximately equal to the stringer pitch (Fig. 2c).

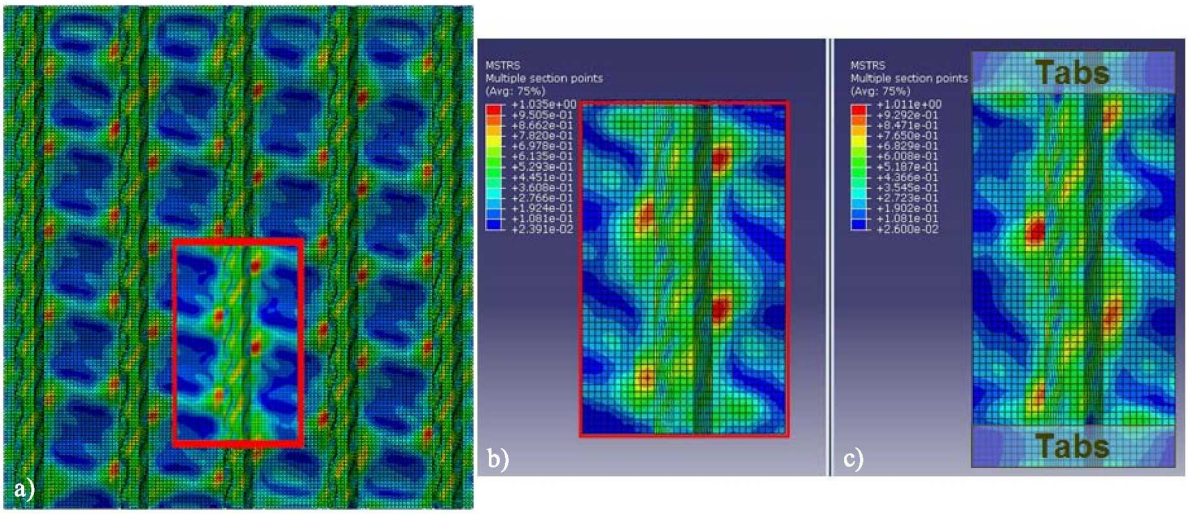

Figure 2. Maximum stress contour plots for a) multi-stringer panel; b) sub-unit of the multi-stringer panel; c) SSC specimen.

As can be observed in Fig. 2, the distribution of maximum stress criterion for the outer ply of the laminates is similar between the multi-stringer panel and the single-stringer specimen. Discrepancies are more pronounced in the areas close to the external edges, while no significant effects are observed in proximity of the stringer foot. In any case, the highest values for the maximum stress failure index are observed in the stringer foot area, where similar patterns are obtained for the single- and multi-stringer configurations. The longitudinal distance between the critical areas is about 120 *mm* for the multi-stringer panel, while it is 115 *mm* for the SSC specimen.

It is important to note that, for experimental simplicity, the longitudinal edges of the SSC specimen are free while the rotations along the corresponding locations of the multi-stringer structure are approximately subjected to symmetry constraints. Moreover, the surrounding structure has the effect of elastically restraining the in-plane motion of the panel, resulting in a membrane stress distribution that is not exactly the same of that one developed in the case of free edges.

III. Test Procedure

Six SSC specimens were manufactured and tested in compression until collapse. In three of the specimens, a Teflon insert was introduced between skin and stringer to assess the effect of initial defects on the residual strength. The insert is 20 *mm* long, and is placed between the skin and the stringer on one of the two stringer flange, centrally located respect to the specimen length, as shown in Fig. 3.

The specimens were encased in potting at the two ends by means of two 30 *mm*-long tabs cast with a mixture of epoxy resin and aluminum powder. The tabs ensure a uniform distribution of the load during the tests.

The specimens were tested under axial compression in displacement control using a MTS dynamic testing system (810 Test Star Iis). Axial load and displacement were measured by the testing system. However, an LVDT transducer was added to measure directly the shortening of the specimen between the end tabs.

Up to collapse, the responses of all the specimens tested were very similar. However, the path of the stringer crippling fracture and the amount of fiber pullout that was observed after the collapse varied somewhat among the specimens. Two typical phases of the structural response before collapse are shown in Fig. 4 for a panel with a Teflon insert. The prebuckling response is characterized by a linear force-displacement response, with a stiffness of about 45 *kN/mm*. At approximately 10 *kN*, the skin of the specimen buckles and the deformation becomes nonlinear. The initial buckling mode of the skin is characterized by three half-waves along the longitudinal direction. The deflection of the skin becomes more visible as the load is increased. Fig. 4a shows the specimen at a load level of 15 *kN*. At this load, the stringer is still stable and does not present any out-of-plane displacements. At approximately 30 *kN*, the stringer webs undergo local buckling, as can be observed in Fig. 4b. In addition, the number of half-waves along the edge of the skin increases from 3 to 5. Since the stringer has a closed section, the local buckling of the webs does not lead to an immediate collapse and the structure can withstand higher loads through internal stress redistribution. The stringer crown remains undeformed until collapse. Finally, collapse occurs suddenly and without visual or acoustic indications of the impending fracture. Two dominant failure mechanisms were observed in all the collapsed panels: stringer crippling and skin/stringer delamination.

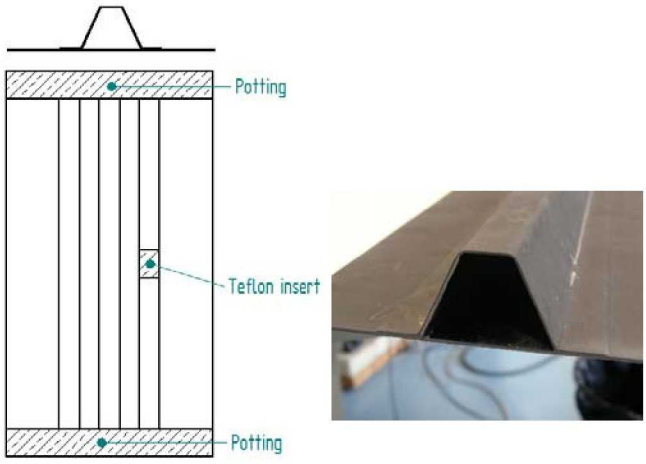

Figure 3. Configuration of SSC specimen and close-up of hat stiffener.

Crippling of the stringer is characterized by a fracture that travels across the stringer width, including the flanges of the stringer. The fracture can run across the stringer in a perpendicular direction or at an angle of approximately 45°. Fiber pullouts from the outer ply of the skin can be observed in most of the panels. The second major failure mechanism is skin/stringer separation. As it can be seen in Figs. 5a (without Teflon insert) and 5b (with Teflon insert), both of these damage modes occur in specimens with or without embedded delaminations.

The postbuckling response and failure modes for nominally pristine specimens and specimens with embedded delaminations were apparently identical. However, the nominally pristine specimens collapse at an average load of 41 *kN*, while those with an embedded delamination collapse at an average load of about 36 *kN* (a 12% reduction).

Small differences can be observed between the specimens. The specimen without a Teflon insert (Fig. 5a) presents a stringer crippling with a fracture oriented at 45°. The fracture at the flanges is at 90° to the stringer, and fiber pullouts can be identified at various locations along the stringer. In Fig. 5b the collapse of a pre-damaged panel is shown. In this case the crippling fracture of the stringer is approximately at the mid-length of the specimen and runs across the stringer at a 90° angle. Although the number of specimens that have been tested so far is

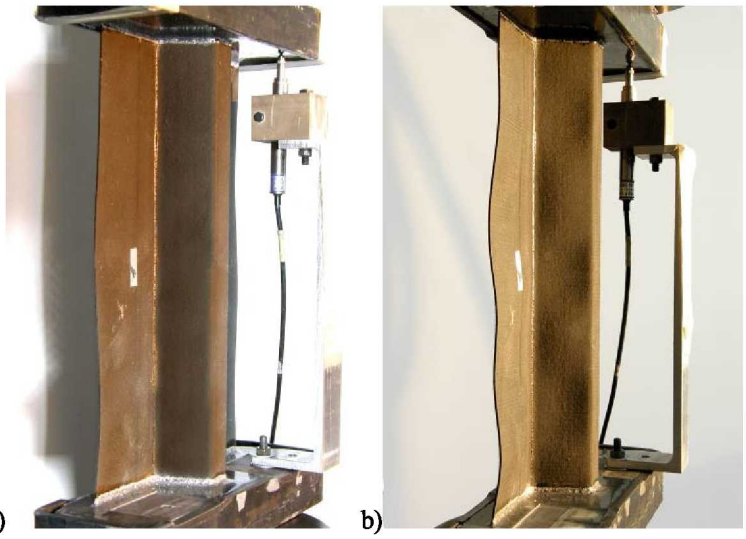

Figure 4. Structural response of a single-stringer specimen with Teflon insert at two load levels: a) 15 *kN*; b) 35 *kN*.

limited, it appears that the different modes of crippling of the stringer are obtained independently of the presence or absence of a Teflon insert.

Fiber damage was generally not found in the skins of most specimens. However, in the specimen shown in Fig. 5c, a crack can be observed in the skin on the side where the Teflon insert was placed. The cause of these fiber fractures is probably the inertial forces that result from the dynamic nature of the collapse.

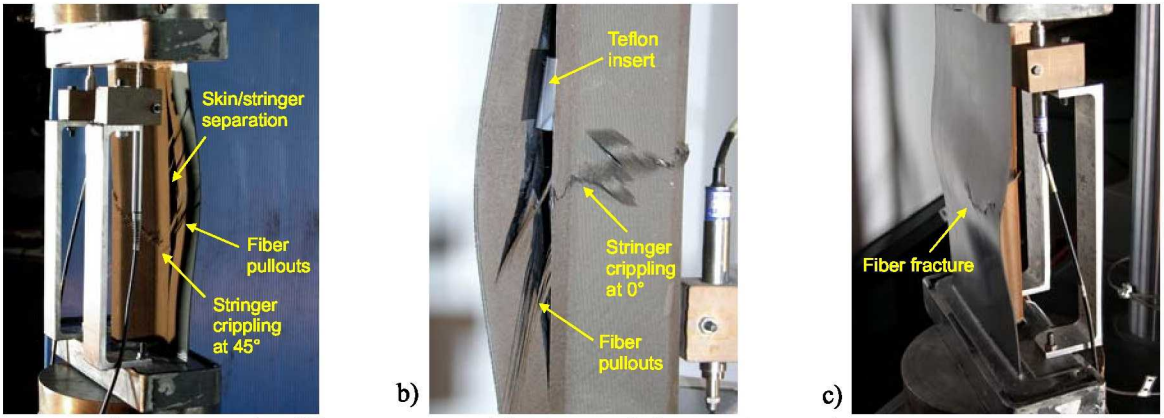

Figure 5. Failure modes in different panels: a) initially pristine specimen; b) specimen with Teflon insert; c) specimen with Teflon insert (back side).

IV. Numerical Analyses

The finite element model of the SSC specimen consists of shell and cohesive elements and is analyzed with the Abaqus finite element code[19]. The skin is composed of a layer of shell elements and the stringer is modeled with another layer. Wall offsets are applied so that the nodes for both shell layers are coincident in the flange sections. The model is defined parametrically. Any dimension of the specimen and the mesh refinement can be modified instantly. The elements have a typical size of 0.8 *mm*, and the total number of degrees of freedom is approximately 710,000. The finite element model of the SSC specimen and its dimensions are shown in Fig. 6.

The two major observed damage modes, skin-stringer separation and intralaminar damage, are taken into account by the model. The skin-stringer separation failure mode is modeled by placing a layer of cohesive elements between the skin and the stringer along the flanges of the stringer. These elements can represent mixed-mode delamination growth with a damage evolution law specified as a bilinear constitutive equation. In the case of the specimen with a Teflon insert, pre-damaged cohesive elements are placed in the area of the Teflon insert.

The initiation and evolution of intralaminar damage is studied using a continuum damage model. The damage mechanisms occurring in the fiber and the matrix are represented by a set of scalar damage. Damage activation functions based on the LaRC04 failure criteria are used to predict the different failure mechanisms occurring at the ply level[3,4].

The analysis of the SSC specimen consists of a thermal analysis followed by a mechanical load. The thermal analysis accounts for the residual thermal stresses that result from contraction between the curing temperature to room temperature. The boundary conditions applied during the thermal step consist in constraining one of the two ends of the specimen while allowing free expansion in the longitudinal direction. The mechanical load consists of the application of an end shortening displacement. The ending tabs of the specimens are simulated by constraining the

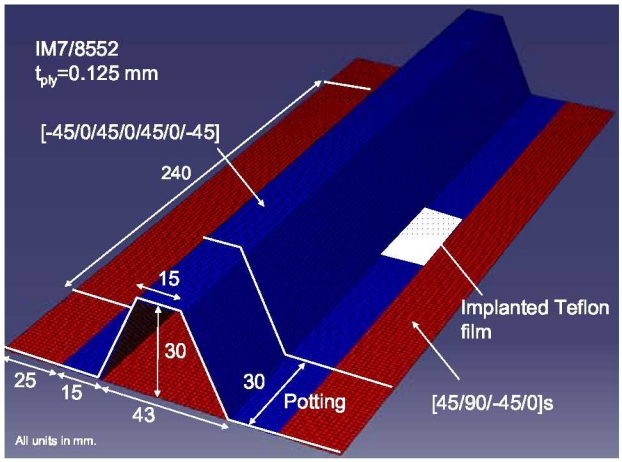

Figure 6. Finite element model and dimensions of the SSC specimen.

translational degrees of freedom of the corresponding nodes.

The analysis is performed as quasi-static using the Newton-Raphson load incrementation technique. However, as the solution approaches the collapse load, the load incrementation procedure becomes unable to find a converged solution. This difficulty is typical of the fracture of structures in which a large amount of strain energy is accumulated before failure. When more strain energy is released by the propagation of a crack than is necessary for fracture, unstable crack propagation occurs during which static equilibrium solutions cannot be found. These difficulties suggest the use of an implicit dynamic analysis, which can overcome the problems related to the convergence of the solution. In order to maximize the efficiency of the procedure, a two-step analysis is adopted. Initially, when convergence issues are not expected, a computationally efficient quasi-static load incrementation step is performed. As damage initiates and convergence problems in the load incrementation procedure arise, the procedure switches to an implicit dynamic solution.

The analysis relies on the material properties obtained from a careful characterization of the material[20]. The engineering moduli and the coefficients of thermal expansion are shown in Table 1. The in-situ ply strengths, which account for the thickness of the ply and its position on the laminate (inner or outer ply), are shown in Table 2. The intralaminar fracture toughnesses shown in Table 3 represent the critical energy release rate for fiber tension, fiber compression, matrix tension, and matrix shear, respectively. These material properties are used in the damage model to set the rate of degradation of the elastic moduli[2-3]. Finally, the interlaminar properties shown in Table 4 are used to define the cohesive law for the skin/stringer interface. These properties consist of the fracture toughnesses in modes I and II, their corresponding strengths, and the B-K mode-mixity parameter that is obtained experimentally[4].

Table 1. Engineering Properties[20] - IM7/8552

E_{11} (*GPa*)	E_{22}(*MPa*)	G_{12}(*MPa*)	ν_{12}	α_1 (*1/°C*)	α_2 (*1/°C*)
150	9080	5290	0.32	-5.5E-6	25.8E-6

Table 2. Ply Strengths[20]- IM7/8552 (*MPa*)

	XT	XC	YT	YC	SL
Single ply	2323	1200	160.2	199.8	130.2
Double or outer ply	2323	1200	101.4	199.8	107.0

Table 3. Ply Fracture Toughnesses[20] - IM7/8552 (*N/mm*)

GF(+)	GF(-)	GMI	GMII
81.5	106.3	0.277	0.788

Table 4. Interlaminar Properties[20] - IM7/8552

GI_c (*N/mm*)	GII_c (*N/mm*)	s_{zz} (*MPa*)	s_{xz} (*MPa*)	B-K
0.277	0.788	50	100	1.6

Figure 7a illustrates the predicted response phases for a nominally pristine specimen at different load levels. In the first phase of the analysis, the specimen exhibits a linear response with a single-wave out-of-plane deformation mode along the free edge of the skin (Point A). At an applied load of 7.5 *kN*, Point B corresponds to the first buckling load, which affects only the skin. Three half-waves are observed along the longitudinal direction. Stringer buckling is predicted at a load of 23.6 *kN* (Point C). Shallow buckles become visible on the two webs of the stringer which form into a series of inclined half-waves. The crown of the stringer remains stable, and the stringer can continue sustaining higher loads. At point D, which corresponds to 38.5 *kN*, skin/stringer separation initiates near the center of the stringer at a location of a flange where the out-of-plane displacements are most negative (blue areas in Fig. 7b). The initiation of separation also corresponds with the peak load of the specimen. Point E represents a state past peak load. Here the specimen has collapsed, and the skin and stringer are separated over a large region of the flanges. The skin is no longer supported by the stringer and its deformed shape is composed of a single irregular longitudinal half-wave.

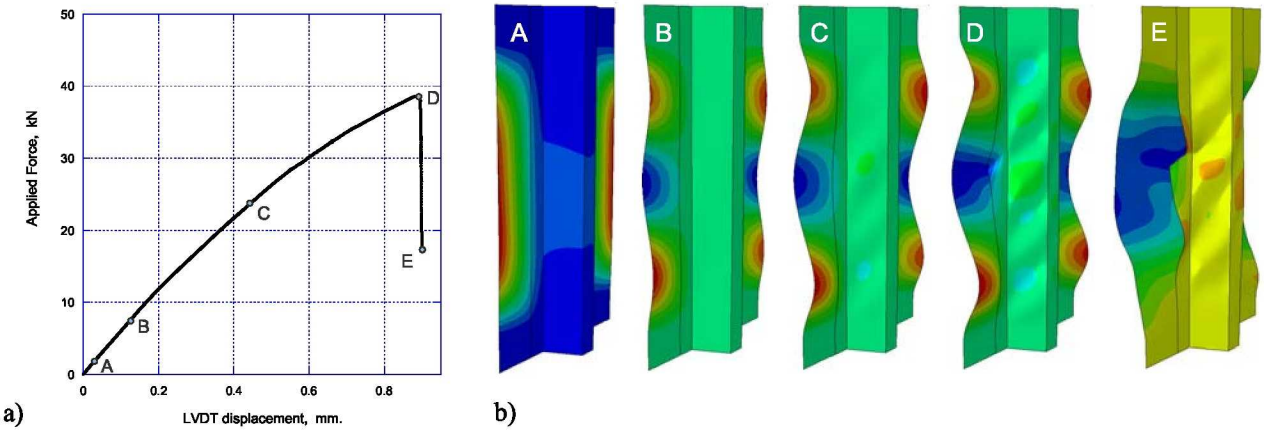

Figure 7. Analysis of the nominally pristine specimen: a) load-displacement curve; b) out-of-plane response.

Figure 8 is a fringe plot illustrating the location of the scalar damage variables related to fiber and matrix damage in compression at three representative load points along the force-displacement curve. At point A, which corresponds to a load of 37 *kN*, fiber damage has initiated at three different locations along the stringer (Fig. 8c). As it can be observed in Fig. 8d, the areas with matrix damage are significantly more extensive than those with fiber damage and they have developed along three different paths inclined at 45°. At point B, corresponding to a state past peak load, a region of fiber damage concentration is formed on one side of the stringer, while the matrix damage extends also into the skin. At point C, fiber fractures are predicted (red fringe) at the corner between the left web of the stringer and its corresponding flange. Fiber damage can also be identified at other locations of the stringer. Matrix damage, on the other hand, is highly diffused, and covers the stringer as well as large areas of the skin.

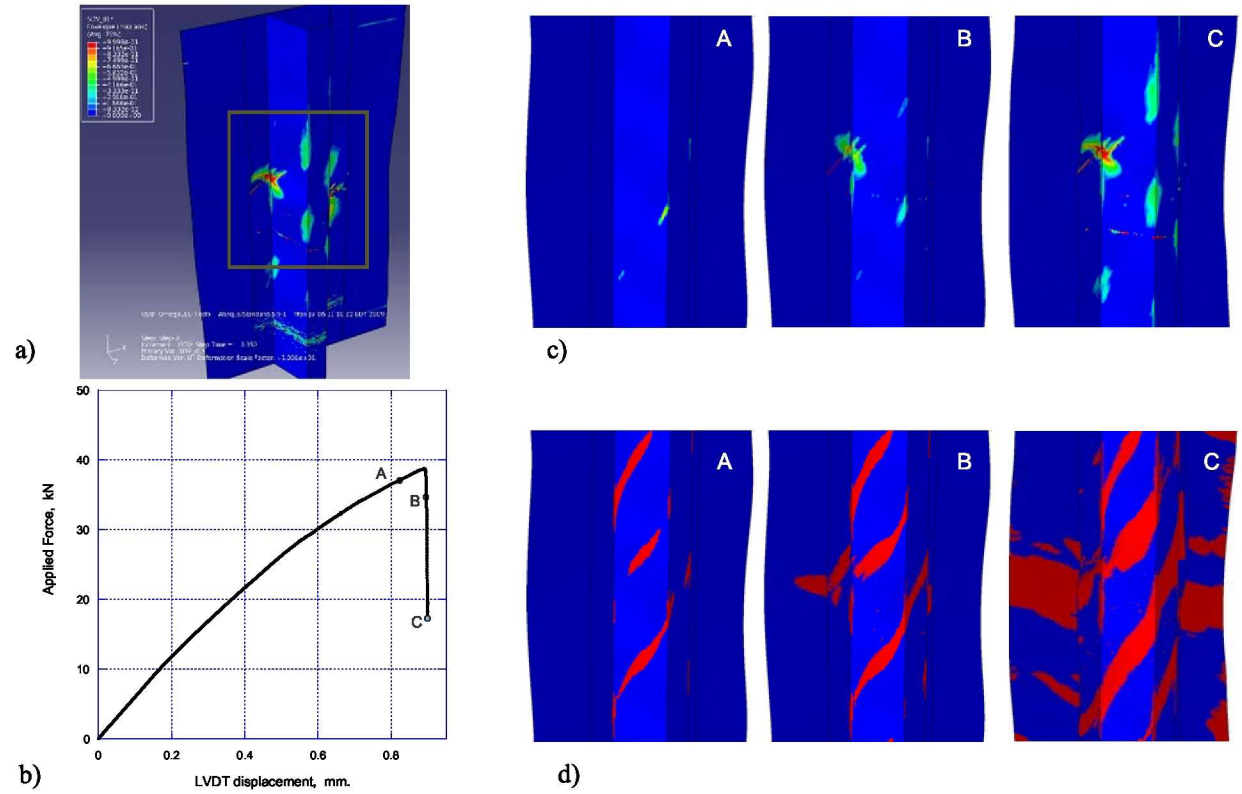

Figure 8. Analysis of the nominally pristine specimen: a) damaged area on the specimen; b) force-displacement curve; c) fiber damage; d) matrix damage.

The evolution of the skin/stringer separation is shown in detail in Fig. 9. The color fringes on the edge views shown in Fig. 9b correspond to regions with fiber damage. The initiation of delamination at load point A corresponds to the peak load, and its propagation occurs during the collapse of the specimen. The analysis predicts a clear separation of the skin and stringer, as shown for load point E.

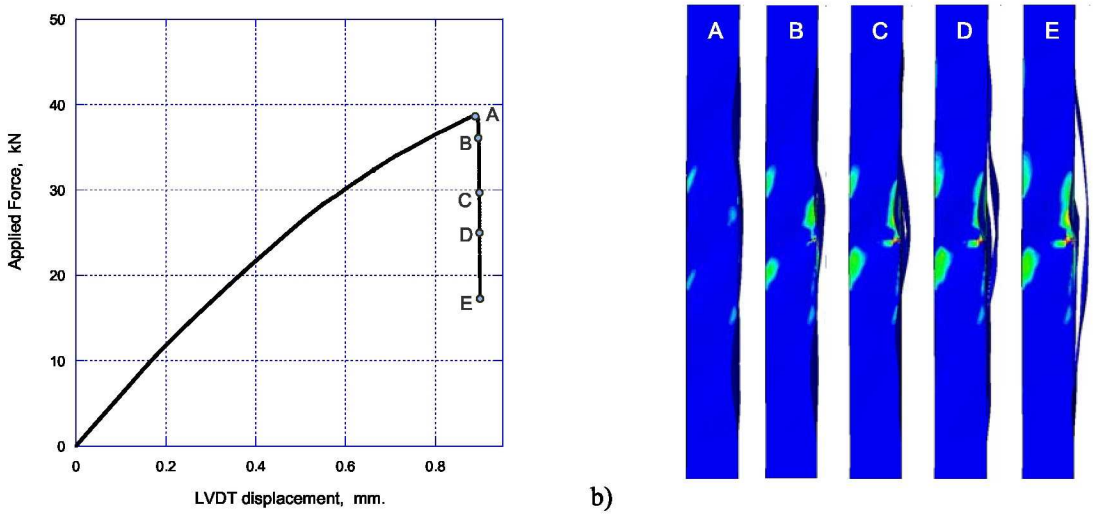

Figure 9. Analysis of the nominally pristine specimen: a) load-displacement curve; b) skin/stringer separation (side view).

V. Numerical – Experimental Comparison

The experimental and numerical results are compared in terms of structural response, damage mechanisms and collapse loads. Fig. 10 reports the force-displacement curves obtained for a typical test specimen without a Teflon insert and another with an insert as well as the corresponding predictions. The numerical results exhibit a slightly higher stiffness than the experimental measurements, probably due to a small sliding of the tabs in the initial loading phase.

At load levels greater than 25 *kN* the experimental force-displacement response curves exhibit more nonlinearities than the corresponding numerical predictions. Higher loads are obtained for the numerical results at the same values of imposed displacement. One of the possible reasons for this effect is related with the nonlinearity of the compression modulus E_{11}, which is not taken into account in the numerical model.

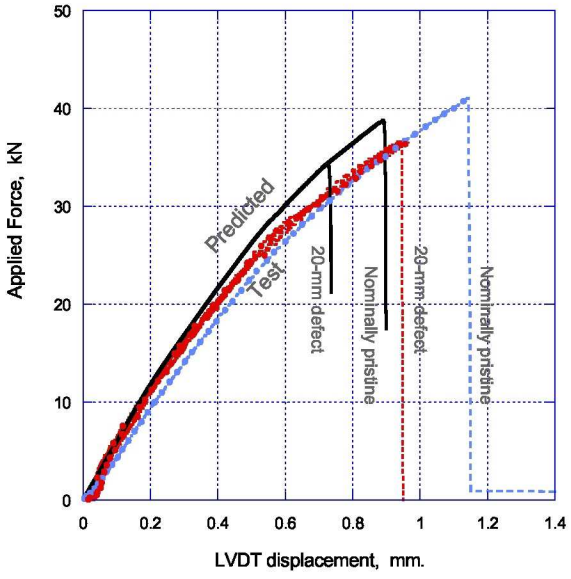

Figure 10. Numerical and experimental force - displacement curves.

A comparison of the predicted and measured deformation shapes for nominally pristine specimens immediately before collapse is shown in Fig. 11. It can be observed that the predicted deformation mode, including the number of half-waves in both the skin and the stringer, correlates well with the experimental observations.

The predicted peak load of the specimen without a Teflon insert is equal to 39 *kN*, which is 5 % lower than the 41 *kN* recorded from the experiment. The predicted peak load for the panel with a Teflon insert is 34 *kN*, which is 5.5 % lower than the 36 *kN* load obtained experimentally.

The fact that the peak loads predicted for specimens with and without Teflon inserts is lower than the experimental values could be attributed to the difference between the interfacial properties of a standard fracture specimen and those of a skin/stringer interface. The interfacial properties used in the present model are the ones obtained from standard fracture toughness tests such as the Double Cantilever Beam and the Mixed-Mode Bending tests. These standard tests are performed using unidirectional material. It has been shown in the literature that the fracture toughness of interfaces other than 0°/0° can be as much as five times greater than obtained from standard tests[21-23]. Secondly, toughening mechanisms such as fiber bridging cause an increase in the fracture toughness. This so-called "R-curve effect" is disregarded in standard tests. Finally, Teflon inserts used as delamination initiators induce a resin-rich zone at the crack tip that increases the initial fracture toughness. These three combined effects tend to increase the fracture toughness compared to the standard properties and their use in the present model would increase the predicted peak loads. Further research is needed to determine the correct values of these interface properties.

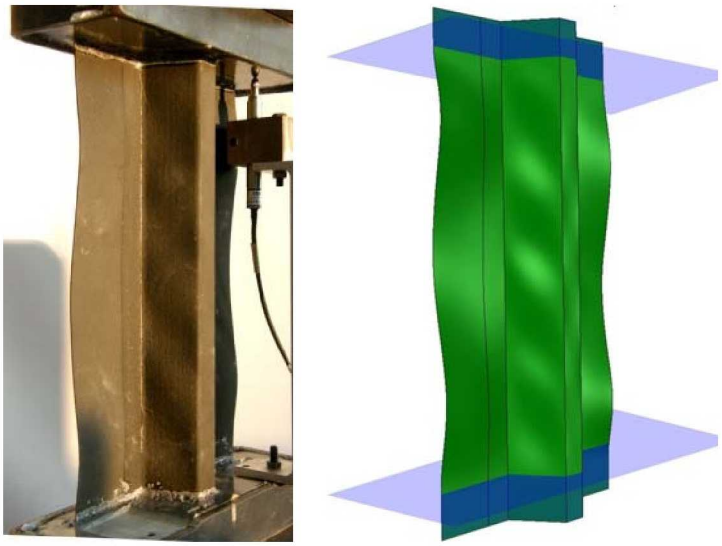

Figure 11. Comparison between experimental and numerical postbuckling deformed shapes.

A comparison between the crippling fracture observed in the test and predicted by the analysis is shown in Fig. 12. The test specimen displays a transverse fracture that crosses the overall stringer. Similarly, the numerical model presents a fracture that is almost transverse on the stringer foot and lateral webs, but is oriented at about 45° on the top crown. Some partial fiber damage is predicted in areas away from the crippling zone that is not apparent in the test specimen.

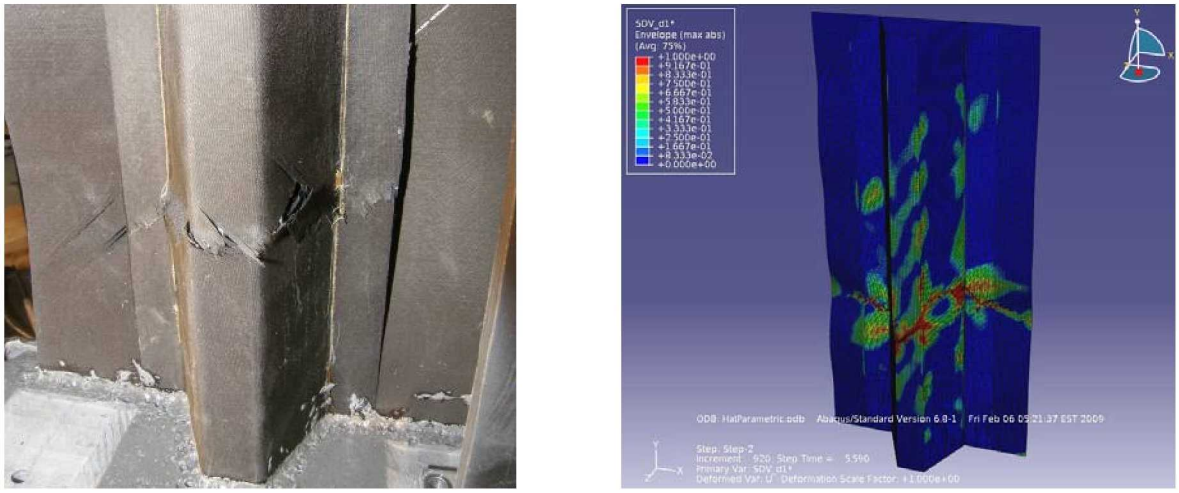

Figure 12. Comparison between experimental and numerical collapse modes.

VI. Conclusions

A single stringer specimen is proposed to investigate experimentally and numerically the postbuckling response of hat-stiffened composite panels and to validate a progressive damage analysis model. The sizing of the specimen was obtained by identifying patterns of predicted failure indices in a multi-stringer panel. The dimensions of a single-stringer specimen with a similar failure index pattern and postbuckling response was obtained by trial-and-error. The use of a relatively small single-stringer panel allows the use of detailed finite element analyses that account for intralaminar and interlaminar damage mechanisms. In addition, the use of single-stringer specimens for the assessment of the damage tolerance of multi-stringer designs minimizes the complexity and the cost of the experimental tests.

Six specimens, with and without a Teflon insert, have been tested under compression until collapse, and two main failure mechanisms were identified: stringer crippling and skin/stringer delamination.

The numerical analyses were performed using ABAQUS with a model capable of capturing the two main mechanisms. Cohesive elements were introduced to study skin/stringer separation, and a continuum damage model was used for the prediction of intralaminar damage. The computational efficiency of the numerical analyses was maximized by combining quasi-static and implicit dynamic procedures. The results indicate good correlation with the experimental data in terms of load-displacement response in the postbuckling range until a load of approximately two times the buckling load. A very satisfactory agreement is found in the predicted collapse loads, differing from the experimental measurements by less than 6%. The analyses also accurately predict the influence of the embedded Teflon inserts on the specimen strength, which reduce the collapse load by approximately 12%. Numerical analyses offered also detailed insight on the intralaminar failure mechanisms. The damage model properly represents the stringer crippling, which is characterized by a fracture that traverses the stringer width. Skin/stringer separation is correctly predicted by the numerical analyses by a clear separation of the skin from the stringer in a mode similar to the one obtained experimentally.

Acknowledgments

Carlos G. Dávila would like to thank the NASA Langley Office of Education for the Floyd Thomson Fellowship that allowed him to spend a sabbatical year of research at Politecnico di Milano. The authors would also like to thank Paolo Rubini and Alessandro Maggiolini of Politecnico di Milano for their contribution to the manufacturing and experimental activities.

References

[1]Lapczyk, I., Hurtado, J. A., "Progressive Damage Modeling in Fiber-Reinforced Materials," *Composites: Part A*, Vol. 38, No. 11, 2007, pp. 2333-2341.

[2]Basu, S., Waas, A. M., Ambur, D. R., "Prediction of Progressive Failure in Multidirectional Composite Laminated Panels," *International Journal of Solids and Structures*, Vol. 44, No. 9, 2007, pp. 2648-2676.

[3]Maimí, P., Camanho, P. P., Mayugo, J. A., Dávila, C. G., "A Continuum Damage Model for Composite Laminates: Part I - Constitutive Model," *Mechanics of Materials*, Vol. 39, No. 10, 2007, pp. 897-908.

[4]Maimí, P., Camanho, P. P., Mayugo, J. A., Dávila, C. G., "A Continuum Damage Model for Composite Laminates: Part II - Computational Implementation," *Mechanics of Materials*, Vol. 39, No. 10, 2007, pp. 909-919.

[5]Turon, A., Camanho, P. P., Costa, J., Dávila, C. G., "A Damage Model for the Simulation of Delamination in Advanced Composites Under Variable-Mode Loading," *Mechanics of Materials*, Vol. 38, No. 11, 2006, pp. 1072-1089.

[6]Camanho, P. P., Dávila, C. G., de Moura, M. F. S. F., "Numerical Simulation of Mixed-Mode Progressive Delamination in Composite Materials," *Journal of Composite Materials*, Vol. 37, No. 16, 2003, pp. 1415-1438.

[7]Dávila, G. C, Camanho, P. P., Turon, A., "Effective Simulation of Delamination in Aeronautical Structures using Shells and Cohesive Elements," *Journal of Aircraft*, Vol. 45, No. 2, 2008, pp. 663-672.

[8]Williams, G. J., Mikulas, M. M., "Analytical and Experimental Study of Structurally Efficient Composite Hat-Stiffened Panels Loaded in Axial Compression," *16th AIAA/ASME/SAE Structures, Structural Dynamics, and Materials Conference,* Denver, Colorado, USA, 27-29 May 1975, AIAA 75-754.

[9]Meeks, C., Greenhalgh, E., Falzon, B. G., "Stiffener Debonding Mechanisms in Post-Buckled CFRP Aerospace Panels," *Composites: Part A,* Vol. 36, No. 7, 2005, pp. 934-946.

[10]Falzon, B. G., Stevens, K. A., Davies, G. O., "Postbuckling Behaviour of a Blade-Stiffened Composite Panel Loaded in Uniaxial Compression," *Composites: Part A,* Vol. 31, No. 5, 2000, pp. 459-468.

[11]Abramovich, H., Grunwald, A., Pevsner, P., Weller, T., David, A., Ghilai, G., Green, A., Pekker, N., "Experiments on Axial Compression Postbuckling Behavior of Stiffened Cylindrical Composite Panels," *44th AIAA/ASME/ASCE/AHS Structures, Structural Dynamics and Material Conference,* Norfolk, Virginia, USA, 7-10 April 2003, AIAA 2003-1793, 2003.

[12]Zimmermann, R., Klein, H., Kling, A., "Buckling and Postbuckling of Stringer Stiffened Fibre Composite Curved Panels - Tests and Computations," *Composite Structures*, Vol. 73, No. 2, 2006, pp. 150-161.

[13]Abramovich H., Bisagni C., Cordisco P., "Post-Buckling Test Simulation of a Stiffened Composite Panel," *48th AIAA/ASME/ASCE/AHS/ASC Structures, Structural Dynamics, and Materials Conference,* Honolulu, Hawaii, USA, 23-26 April 2007, AIAA 2007-2126.

[14]Abramovich, H., Weller, T., Bisagni, C., "Buckling Behavior of Composite Laminated Stiffened Panels Under Combined Shear-Axial Compression," *Journal of Aircraft*, Vol. 45, No. 2, 2008, pp. 402-413.

[15]Cordisco, P., Bisagni, C., "Effect of Cyclic Buckling Under Combined Loading on Pre-Damaged Composite Stiffened Box," *50th AIAA/ASME/ASCE/ASC Structures, Structural Dynamics, and Materials Conference*, Palm Springs, California, USA, 4-7 May 2009, AIAA 2009-2498.

[16]Bisagni, C., "Progressive Delamination Analysis of Stiffened Composite Panels in Post-Buckling," *47th AIAA/ASME/ASCE/ASC Structures, Structural Dynamics, and Materials Conference,* Newport, Rhode Island, USA, 1-4 May 2006, AIAA 2006-2178.

[17]Orifici, A. C., de Zarate Alberdi, I. O., Thomson, R. S., Bayandor, J., "Compression and Post-Buckling Damage Growth and Collapse Analysis of Flat Composite Stiffened Panels," *Composites Science and Technology,* Vol. 68, No.15-16, 2008, pp. 3150-3160.

[18]Orifici A. C, Thomson R.S., Degenhardt R., Bisagni C., Bayandor J., "A Finite Element Methodology for Analysing Degradation and Collapse in Postbuckling Composite Aerospace Structures," *Journal of Composite Materials,* Vol. 43, No. 26, 2009, pp. 3239-3263.

[19]Abaqus 6.9 User's Manual, Dassault Systèmes, Providence, RI, USA, 2008.

[20]Camanho, P.P., Maimí, P., and Dávila, C.G., "Prediction of Size Effects in Notched Laminates Using Continuum Damage Mechanics," Composites Science and Technology, Vol. 67, No. 13, 2007, pp. 2715-2727.

[21]Andersons, J., and König, M., "Dependence of Fracture Toughness of Composite Laminates on Interface Ply Orientations and Delamination Growth Direction," *Composites Science and Technology*, Vol. 64, No. 13-14, 2004, pp. 2139-2152.

[22]Pereira, A.B., and de Morais, A.B., "Mode I Interlaminar Fracture of Carbon/Epoxy Multidirectional Laminates," *Composites Science and Technology*, Vol. 64, No. 13-14, 2004, pp. 2261-2270.

[23]Schön, J., Nyman, T., Blom, A., and Ansell, H., "A Numerical and Experimental Investigation of Delamination Behaviour in the DCB Specimen," *Composites Science and Technology*, Vol. 60, No. 2, 2000, pp. 173-184.